The Experimental Electron Density Distribution in the Complex of (*E*)-1,2-Bis(4-pyridyl)ethylene with 1,4-Diiodotetrafluorobenzene at 90 K

Riccardo Bianchi,* Alessandra Forni, and Tullio Pilati[a]

Abstract: The experimental electron density of the donor–acceptor complex of (*E*)-1,2-bis(4-pyridyl)ethylene (bpe) with 1,4-diiodotetrafluorobenzene (F_4DIB) at 90 K has been determined with the aspherical atom formalism and analyzed by means of the topological theory of molecular structure. The bpe and F_4DIB molecules are connected by intermolecular I···N bonds into infinite 1D chains. F···H bonds link these chains together to form the crystal assembly. The topological analysis reveals that the C–I bond is of the "closed shell" type. Its bond-critical properties run parallel to those found in metal–metal and metal–ligand bonds of organometallic compounds. The integrated net charges show that the I···N halogen bond has an essentially electrostatic nature. F···F, F···C, and C···C intermolecular interactions, for which a bond path was found, contribute to reinforce the crystal structure.

Keywords: donor–acceptor systems · electron density · iodine · supramolecular chemistry · topological analysis

Introduction

In previous papers,[1–8] the effective and reliable role of halogen bonding (i.e. the tendency of halogen atoms to interact with Lewis bases) to assemble molecules into supramolecular architectures has been demonstrated. The relevance of halogen bonding in the self-assembly of structurally different molecules extends to rather different fields (biopharmacology, synthetic chemistry, purification processes, and materials science), that is, to all the fields in which design and manipulation of aggregation processes play a key role. The neighboring group effect on the electron-accepting properties of a given halogen atom has been widely recognized and the inductive effect from substituents has been observed from the donor side as well.[4] Electrostatic effects, polarization, charge transfer, and dispersion contributions are important in the interaction,[9] and numerous properties characterizing the interaction have analogies with those of the hydrogen bond.[1, 2, 4]

To provide insight into the intermolecular interactions between halogens and electronegative atoms, we focused our attention on a complex formed between a Lewis base and an iodoperfluoro compound. To this end, we present here an X-ray study at 90 K of the multipole-refined electron density[10] of the complex between (*E*)-1,2-bis(4-pyridyl)ethylene (bpe) and 1,4-diiodotetrafluorobenzene (F_4DIB) in terms of its topological properties.[11] The experimental results are also compared with accurate theoretical all-electron calculations. bpe·F_4DIB is a charge-transfer complex and can be considered a simple structural model that is useful in crystal engineering projects, for example, in the construction of nanoporous polydiacetylenes and polytriaryldienes.[12] The structural analysis at room temperature was published elsewhere.[3]

[a] Dr. R. Bianchi, Dr. A. Forni, Dr. T. Pilati
CNR—Istituto di Scienze e Tecnologie Molecolari
via Golgi 19, 20133 Milano (Italy)
Fax: (+39) 02 50314300
E-mail: riccardo.bianchi@istm.cnr.it

Supporting information for this article is available on the WWW under http://www.wiley-vch.de/home/chemistry/ or from the author.

Results and Discussion

Structural properties: The complex bpe·F_4DIB crystallizes in the $P\bar{1}$ space group. The unit cell consists of one bpe molecule and one F_4DIB molecule, both lying on a center of symmetry. The low-temperature structure does not undergo large variations with respect to the room-temperature structure.[3] Bond lengths, bond angles, and selected intermolecular contacts (almost within the sum of the van der Waals radii) from the final multipole refinement (POP + CUM) are reported in Table 1.

The crystal structure consists of infinite linear chains in which both ends of the bpe donor molecules are halogen-bonded to both ends of the F_4DIB acceptor molecules (see Figure 1). The I···N distance, 2.7804(8) Å, is slightly shorter than the corresponding room temperature value, 2.810(5) Å,[3] and significantly shorter than the sum of the van der Waals radii, 3.5 Å.[13] The bpe and F_4DIB molecules are well-aligned along the chains, as indicated by the C–I···N and the I···N···

Table 1. Bond lengths, bond angles, and selected intermolecular contacts from the POP + CUM refinement. The asterisk indicates atomic interaction where a bond path was found.[a]

Intramolecular bond lengths [Å]		Intramolecular bond angles [°]		Intermolecular contacts [Å]	
C7−I	2.0969(7)	I-C7-C8	121.32(4)	I···N^{III}	2.7804(8)*
C7−C8	1.3897(8)	I-C7-C9	121.74(4)	I···C5^{III}	3.6246(10)
C7−C9	1.3885(9)	C8-C7-C9	116.94(6)	I···C4^{III}	3.6933(9)
C8−C9^{I}	1.3881(9)	C7-C8-F1	119.85(6)	F1···H3^{IV}	2.44(1)*
C8−F1	1.3402(10)	C7-C8-C9^{I}	121.65(5)	F1···H5^{V}	2.90(2)*
C9−F2	1.3399(9)	F1-C8-C9^{I}	118.50(6)	F1···C3^{IV}	3.1495(10)
C1−C1^{II}	1.3532(13)	C7-C9-F2	120.15(6)	F2···H1^{VI}	2.49(2)*
C1−C2	1.4635(10)	C7-C9-C8^{I}	121.41(5)	F2···H6^{VI}	2.74(2)*
C2−C3	1.4003(10)	F2-C9-C8^{I}	118.43(6)	F2···F2^{VII}	3.0326(14)*
C2−C6	1.3999(9)	C1^{II}-C1-C2	124.49(8)	F2···C4^{VIII}	3.2927(13)*
C3−C4	1.3867(11)	C1-C2-C3	123.48(6)	C2···C8^{II}	3.3791(11)*
C6−C5	1.3888(11)	C1-C2-C6	119.45(6)	C4···C4^{III}	3.4688(13)*
C4−N	1.3410(11)	C3-C2-C6	117.08(6)		
C5−N	1.3363(11)	C2-C3-C4	119.38(6)		
C1−H1	1.07(2)	C3-C4-N	123.39(7)		
C3−H3	1.01(2)	C4-N-C5	117.35(7)		
C4−H4	1.05(2)	N-C5-C6	123.45(7)		
C5−H5	0.99(2)	C2-C6-C5	119.35(7)		
C6−H6	1.02(2)	H1-C1-C2	118.0(9)		
		H1-C1-C1^{II}	117.6(9)		
		C2-C3-H3	115.2(10)		
		H3-C3-C4	125.4(10)		
		C3-C4-H4	118.8(9)		
		H4-C4-N	117.8(9)		
		N-C5-H5	118.1(10)		
		H5-C5-C6	118.3(10)		
		C2-C6-H6	125.3(9)		
		C5-C6-H6	115.3(9)		

[a] The Roman numerals refer to the following symmetry operations: I: $-x, -y, -z$; II: $-x, -y, -1-z$; III: $-1-x, 1-y, -1-z$; IV: $1+x, y, z$; V: $-x, 1-y, -1-z$; VI: $-1+x, y, 1+z$; VII: $-1-x, -y, -z$; VIII: $x, y, 1+z$.

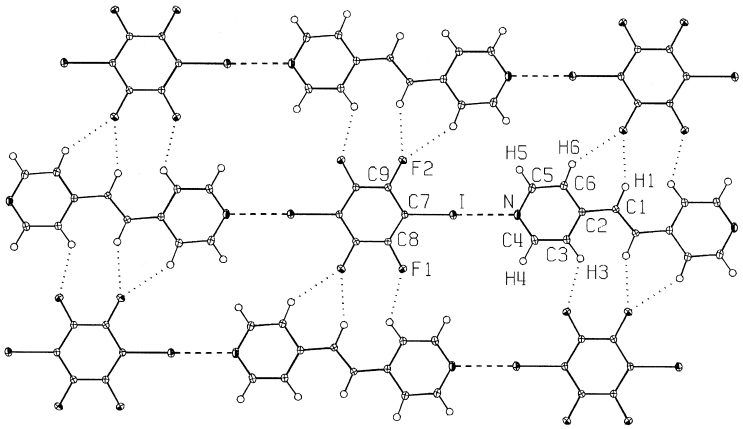

Figure 1. Crystal packing view along c with atom numbering scheme in the plane defined by I, $I_{-x,-y,-z}$ and F2. Dashed lines: I···N interactions; dotted lines: F···H interactions.

C2 angles, 179.32(3) and 177.20(3)°, respectively. Adjacent chains are linked together by C−H···F hydrogen bonds[14] to form slightly corrugated planes. In particular, F1 is hydrogen-bonded to H3, and F2 forms a bifurcate bond with H1 and H6 (C-H···F angles equal to 127(1), 149(2) and 137(2)°, respectively). These corrugated planes are connected to each other by weaker hydrogen bonds (C5−H5···F1 angle equal to 112(1)°) and by π−π interactions involving pyridine and diiodofluorobenzene rings. The angle between the least-squares planes through the rings is 6.96(2)° and the average distance of the pyridine atoms from the least-squares plane through the diiodofluorobenzene ring is 3.379(1) Å.

Difference electron densities: The residual map (based on $F_{observed} - F_{multipole}$) shows no significant features (Figure 2a) and the largest peak (close to the iodine nucleus) is 0.26(7) e Å^{-3}. The average standard deviation of the total density, which is representative of the error in the difference density at positions away from the nuclei, is 0.1 e Å^{-3}. The fact that all the features in the residual map are below 3σ (except for the negative hole of $-0.51(8)$ e Å^{-3} close to the I nucleus) indicates that the POP + CUM model used in the refinement is adequate.

The deformation density map (Figure 2b, based on $F_{observed} - F_{IAM}$, where IAM indicates the independent atom model) shows features of the observed electron accumulation resulting from the bonding between the atoms.

We observe a flat peak near to the midpoint of the C−I bond (0.31(6) e Å^{-3}) and maxima between the other bonded atoms. The broad diffuse peak along the ethylene bond is clearly distinguishable from the well-shaped peaks on the C−C and C−N bonds, and the presence of peaks in the lone pair and in the intermolecular regions of the I and F atoms is remarkable.

Topology of the electron density: The topology of the electron density, $\rho(r)$, and its Laplacian, $\nabla^2\rho(r)$, is related to chemical concepts by the quantum theory of atoms in molecules (QTAM).[11] The definition of the chemical bond is based on the existence of a bond critical point (BCP) along a line of maximum density (bond path), linking the nuclei of neighboring atoms. At the BCP, the gradient of density vanishes and the sign of the Laplacian is determined by the relationship, $\nabla^2\rho_b = \lambda_1 + \lambda_2 + \lambda_3$ ($\lambda_1 < 0$, $\lambda_2 < 0$, and $\lambda_3 > 0$ are the three nonzero eigenvalues of the Hessian matrix). The values of λ_1 and λ_2 measure the degree of the $\rho(r)$ contraction towards the BCP, while λ_3 gives the $\rho(r)$ contraction towards

© 2003 WILEY-VCH Verlag GmbH & Co. KGaA, Weinheim
0947-6539/03/0907-1632 $ 20.00+.50/0 *Chem. Eur. J.* **2003**, *9*, No. 7

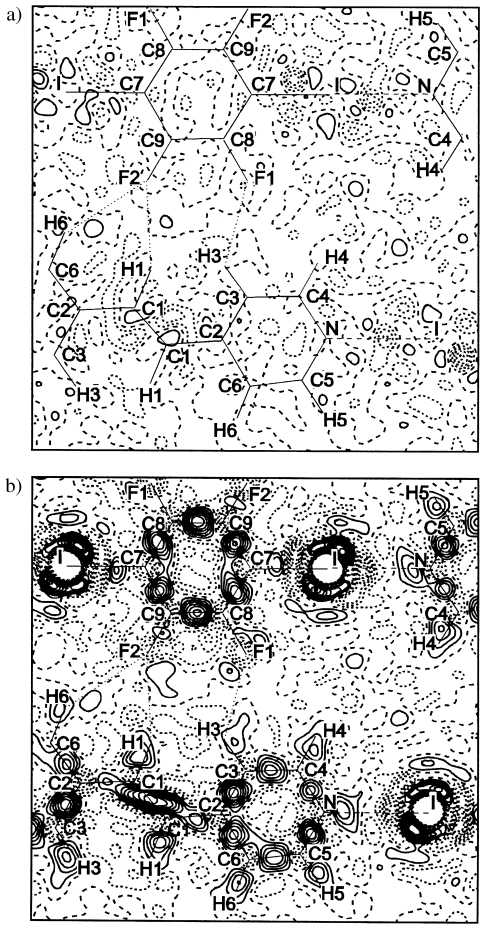

Figure 2. a) Residual density and b) deformation density maps in the least-squares plane defined by the heavy atoms of F_4DIB and bpe$_{1+x,y,z}$ molecules. The contour interval is 0.10 e Å^{-3}. Solid lines: positive contours; short dashed lines: negative contours; wide dashed lines: zero contours.

each of the bonded nuclei. If the electrons are locally concentrated around the BCP and shared by both nuclei (covalent atomic interaction) $\nabla^2\rho_b$ is less than zero. Otherwise, if the electrons are depleted from the BCP and concentrated in each of the atomic basins (closed-shell atomic interaction), $\nabla^2\rho_b$ is greater than zero. Extremes in $\nabla^2\rho(r)$ are labeled by giving the pair of values (ω,σ), in the same way as critical points in $\rho(r)$. ω denotes the rank that is equal to the number of non-zero eigenvalues, σ denotes the signature that is the number of positive eigenvalues minus the number of the negative ones. The number and properties of the local $\nabla^2\rho(r)$ maxima and minima in the valence shell charge concentration (VSCC) of the bonded atoms depend on the linked atoms themselves. Local concentrations and depletions of the electrons in the internuclear space are also connected to the features of the electronic energy distribution.[15] An additional straightforward criterion for the characterization of the chemical bond is provided by the local electronic energy density $E^e_b = G_b + V_b$, where G_b and V_b indicate, respectively, the experimental values of the kinetic and potential energy density at the BCP, and they were calculated from Abramov[16] and Espinosa et al.[17]

The covalent bonds show relatively large values of ρ_b (the value of $\rho(r)$ at the BCP) and large negative values of $\nabla^2\rho_b$. These shared atomic interactions have negative E^e_b, in which the local electronic potential energy V_b dominates. On the contrary, the ionic bonds have relatively low ρ_b and positive E^e_b. Moreover, G_b is slightly greater than $|V_b|$ and the resulting value of E^e_b is close to zero.

For the title complex, the properties of the experimental and theoretical electron density at the BCPs are reported in Table 2 and Table 3.

Figure 3 and Figure 4 show, respectively, the experimental electron density $\rho(r)$ of the bpe·F_4DIB complex and its Laplacian $\nabla^2\rho(r)$ in the least-squares plane defined by the heavy atoms. The Laplacian map shows a shell structure in the valence region of the electron density of each atom.

F_4DIB molecule: The C7–I bond is characterized at the BCP by a relatively low electron density ρ_b of 0.76(1) e Å^{-3} and a positive Laplacian $\nabla^2\rho_b$ of 1.4(2) e Å^{-5} and it is classified as a closed-shell type of atomic interaction. The small magnitudes of the λ_1 and λ_2 curvatures of the density, which are much smaller than the bond parallel curvature (λ_3), are in agreement with a flat $\rho(r)$ on the interatomic surface (see Figure 3). The BCP of the C7–I bond is almost halfway between the atoms, in agreement with their electronegativity. These findings suggest that the C7–I bond has topological properties which appear to be intermediate between those of covalent and ionic bonds, as found for metal–metal and metal–ligand bonds in organometallic compounds.[18–20] In particular, this bond shows almost identical topological features to that determined for the Co–Co bond in the orthorhombic phase of $[Co_2(CO)_6(\mu\text{-}CO)(\mu\text{-}C_4O_2H_2)]$.[20]

The BCPs of the C7–C8 and C7–C9 bonds are somewhat shifted towards the C7 atom with respect to the bond midpoint. This reflects the polarization in the phenyl ring caused by the electron-withdrawing properties of the fluorine atoms bonded to C8 and C9. The polar C–F bonds have BCPs that are closer to the less electronegative carbon atom. The topological values of the C–C and C–F bonds are typical of covalent interactions.

bpe molecule: In this molecule, the C=C double and C–C single bonds, the C–H bonds, and the C–C and C–N aromatic bonds of the pyridine group are present. All these bonds are characterized (Table 2) by high values of ρ_b (av value = 2.13 e Å^{-3}) and large negatives values of $\nabla^2\rho_b$ (average = −19.7 e Å^{-5}), in agreement with those of typical covalent bonds. Despite the fairly large standard deviations, the BCP ellipticities ε on the pyridine ring and on the C1=C1$_{-x,\,-y,\,-1-z}$ double bond (average $\varepsilon = 0.28$), are significantly greater than those on the C1–C2 and C–H bonds (average $\varepsilon = 0.08$), giving a measure of the anisotropy of the bonds. The level of the electron density depletion at the center of the pyridine ring is approximately the same as that determined at the center of the phenyl ring in the F_4DIB molecule. The topological analysis of the Laplacian reveals the sp^2 hybridization of the L-shell structure for the N and C atoms in both the bpe and F_4DIB molecules.

BCPs energetic properties: The kinetic energy density (G_b) and the potential energy density (V_b) at the BCPs were

 © 2003 WILEY-VCH Verlag GmbH & Co. KGaA, Weinheim 0947-6539/03/0907-1633 $ 20.00+.50/0

Table 2. Bond critical point properties from POP + CUM model. R_x = distance between atom X and the BCP; R_e = distance between atoms X and Y. First row: experimental POP + CUM model; second row (italics): theoretical RHF calculations.

X–Y	R_x[Å]	R_x/R_e[Å]	ρ_b[e Å^{-3}]	$\nabla^2\rho_b$[e Å^{-5}]	λ_1[e Å^{-5}]	λ_2[e Å^{-5}]	λ_3[e Å^{-5}]
			intramolecular bond critical points				
C7–I	1.0660	0.51	0.76(1)	1.4(2)	−1.94	−1.42	4.79
	1.0756	*0.51*	*0.81*	*3.8*	*−2.79*	*−2.67*	*9.23*
C7–C8	0.6463	0.47	2.15(4)	−17.9(13)	−17.14	−13.62	12.89
	0.6642	*0.48*	*2.21*	*−24.4*	*−17.40*	*−13.34*	*6.30*
C7–C9	0.6338	0.46	2.06(4)	−17.6(14)	−16.08	−12.95	11.41
	0.6628	*0.48*	*2.21*	*−24.5*	*−17.44*	*−13.37*	*6.27*
C8–C9[I]	0.6924	0.50	2.27(4)	−21.1(11)	−20.72	−13.93	13.58
	0.6940	*0.50*	*2.26*	*−25.8*	*−19.07*	*−13.44*	*6.67*
C8 – F1	0.5161	0.39	1.90(6)	−18.0(27)	−16.25	−14.13	12.35
	0.4270	*0.31*	*1.72*	*11.1*	*−12.89*	*−12.20*	*36.24*
C9 – F2	0.5312	0.40	2.01(2)	−20.0(24)	−18.18	−15.77	14.00
	0.4267	*0.32*	*1.71*	*11.6*	*−12.83*	*−12.13*	*36.54*
C1 – C1[II]	0.6766	0.50	2.59(6)	−24.2(19)	−23.64	−17.32	16.74
	0.6746	*0.50*	*2.32*	*−25.7*	*−18.30*	*−13.13*	*5.78*
C1 – C2	0.7270	0.50	1.82(4)	−13.2(9)	−13.84	−12.07	12.67
	0.7255	*0.50*	*1.94*	*−20.3*	*−14.31*	*−13.36*	*7.37*
C2 – C3	0.7261	0.52	2.18(4)	−19.2(12)	−18.34	−14.96	13.68
	0.7244	*0.52*	*2.16*	*−23.6*	*−16.53*	*−13.79*	*6.69*
C2 – C6	0.7219	0.52	2.07(4)	−17.1(12)	−16.69	−13.12	12.67
	0.7114	*0.51*	*2.16*	*−23.5*	*−16.56*	*−13.74*	*6.79*
C3 – C4	0.7028	0.51	2.25(4)	−21.0(12)	−18.87	−15.22	13.12
	0.6847	*0.49*	*2.21*	*−24.5*	*−17.32*	*−13.77*	*6.56*
C6 – C5	0.6988	0.50	2.21(4)	−20.0(12)	−19.28	−13.83	13.08
	0.6786	*0.49*	*2.22*	*−24.8*	*−17.45*	*−14.05*	*6.65*
C4 – N	0.5579	0.42	2.27(6)	−22.3(25)	−19.86	−15.67	13.19
	0.4428	*0.33*	*2.32*	*−19.5*	*−18.91*	*−17.52*	*16.93*
C5 – N	0.6378	0.48	2.59(5)	−22.5(16)	−23.47	−19.81	20.82
	0.4399	*0.33*	*2.33*	*−18.2*	*−18.93*	*−17.78*	*18.54*
C1 – H1	0.7158	0.67	1.86(7)	−17.6(18)	−19.62	−18.10	20.13
	0.6577	*0.61*	*2.04*	*−28.7*	*−19.45*	*−19.09*	*9.85*
C3 – H3	0.6540	0.65	1.92(7)	−20.1(20)	−20.26	−18.11	18.26
	0.5991	*0.59*	*2.31*	*−37.0*	*−22.63*	*−22.24*	*7.83*
C4 – H4	0.7212	0.69	1.98(7)	−20.1(20)	−21.27	−20.33	21.53
	0.6569	*0.63*	*2.15*	*−32.7*	*−21.61*	*−21.09*	*10.01*
C5 – H5	0.6911	0.70	1.93(8)	−18.1(27)	−21.70	−20.23	23.86
	0.5936	*0.60*	*2.44*	*−42.2*	*−25.08*	*−24.60*	*7.54*
C6 – H6	0.6502	0.64	2.06(7)	−20.9(19)	−20.93	−19.53	19.55
	0.6099	*0.60*	*2.27*	*−35.9*	*−22.24*	*−21.84*	*8.20*
			ring critical points				
C7-C8-C9[I]-C7[I]-C8[I]-C9			0.199(8)	2.78(6)	−0.31	1.26	1.82
			0.126	*3.69*	*−0.28*	*1.95*	*2.02*
C2-C3-C4-N-C5-C6			0.220(6)	3.15(5)	−0.44	1.73	1.87
			0.147	*4.34*	*−0.40*	*2.14*	*2.60*

computed according to Abramov's formula.[16] Their values, as regards the C7–I bond 0.57(1) and −1.05(3) H Å^{-5}, respectively, are quite small and the resulting local energy density E^e_b is slightly negative (−0.47(4) H Å^{-5}). The corresponding "exact" values, as obtained from the ab initio RHF calculations, are 0.64, −1.01, and −0.37 H Å^{-5}. In agreement with what reported for close-shell interactions,[16] our estimate for G_b and V_b is within 11 %.

For all the covalent bonds in the bpe·F_4DIB complex, the large negative E^e_b values (av −3.3 H Å^{-3}) are caused by the larger magnitude of V_b (av −5.2 H Å^{-3}) with respect to G_b (av = 1.9 H Å^{-3}). The corresponding theoretical values are $E^e_b = -2.7$, $V_b = -3.7$, and $G_b = 1.1$ H Å^{-3}. In this case, the relative error of the experimental mean values, with respect to the theoretical ones, is 73 % for G_b and 41 % for V_b. As noted by Abramov, this large disagreement is caused by the approximated formula used in the experimental case. In fact, the mean theoretical values calculated according to Abramov's equation are $V_b = -5.3$ and $G_b = 1.9$ H Å^{-3}.

Intermolecular interactions: Table 3 lists the intermolecular interactions for which a bond path was found. The magnitudes of all the BCP properties in the upper part of Table 3 decrease starting from the I···N to the F1···H5 interaction, clearly suggesting the relative strength of these intermolecular bonds. Moreover, the ρ_b, $\nabla^2\rho_b$, G_b and V_b magnitudes of the I···N bond indicate that this interaction is comparable to an O–H···O hydrogen bond of medium strength.[21]

The equation tested by Espinosa et al. for the calculation of the hydrogen bond energy E_{HB},[22] $E_{HB} = \frac{1}{2}V_b$, gives the strength of the halogen bond as 8.9 kcal mol^{-1}. In spite of the simplicity of this model and of the different pair of interacting atoms, the estimated energy of the I···N bond is close to other experimental and theoretical values. In fact, the

© 2003 WILEY-VCH Verlag GmbH & Co. KGaA, Weinheim
0947-6539/03/0907-1634 $ 20.00+.50/0 *Chem. Eur. J.* **2003**, *9*, No. 7

Table 3. Bond critical point properties of intermolecular interactions for which a bond path was found. First row: experimental POP + CUM model; second row: experimental IAM model. Theoretical RHF calculations, when available, are given in italics.[a]

X···Y	R_x [Å]	ρ_b [e Å^{-3}]	$\nabla^2\rho_b$ [e Å^{-5}]	λ_1 [e Å^{-5}]	λ_2 [e Å^{-5}]	λ_3 [e Å^{-5}]	G_b [(H Å^{-3}]	V_b [(H Å^{-3}]	E^e_b [(H Å^{-3}]
I···N^{I}	1.514	0.236(2)	1.96(2)	−0.68	−0.66	3.30	0.164(1)	−0.191(3)	−0.027(4)
	1.556	0.211	2.60	−0.58	−0.57	3.75	0.182	−0.181	0.001
	1.431	*0.181*	*1.87*	*−0.45*	*−0.42*	*2.74*	*0.132*	*−0.133*	*−0.001*
F1···H3^{II}	1.326	0.071(4)	1.09(2)	−0.27	−0.26	1.62	0.061(1)	−0.045(3)	0.016(3)
	1.319	0.070	1.17	−0.27	−0.25	1.69	0.064	−0.047	0.018
	1.398	*0.054*	*0.92*	*−0.21*	*−0.20*	*1.33*	*0.055*	*−0.045*	*0.010*
F2···H1^{IV}	1.461	0.030(5)	0.66(2)	−0.10	−0.09	0.85	0.032(1)	−0.019(3)	0.012(3)
	1.409	0.039	0.72	−0.14	−0.14	1.00	0.038	−0.026	0.013
	1.433	*0.043*	*0.73*	*−0.17*	*−0.16*	*1.06*	*0.043*	*−0.035*	*0.008*
F2···H6^{V}	1.476	0.030(2)	0.50(2)	−0.10	−0.09	0.68	0.026(1)	−0.016(2)	0.009(3)
	1.487	0.029	0.49	−0.09	−0.07	0.66	0.026	−0.016	0.009
	1.539	*0.024*	*0.47*	*−0.08*	*−0.07*	*0.62*	*0.025*	*−0.017*	*0.008*
F1···H5^{III}	1.565	0.024(2)	0.38(1)	−0.05	−0.03	0.47	0.019(1)	−0.012(1)	0.007(1)
	1.544	0.025	0.40	−0.06	−0.04	0.49	0.020	−0.013	0.008
other intermolecular interactions									
F2···F2^{V}	1.516	0.034(1)	0.60(1)	−0.07	−0.02	0.70	0.031(1)	−0.020(1)	0.011(1)
	1.517	0.034	0.58	−0.07	−0.02	0.67	0.030	−0.019	0.011
F2···C4^{VI}	1.553	0.034(1)	0.43(1)	−0.05	−0.02	0.51	0.023(1)	−0.016(1)	0.007(1)
	1.550	0.030	0.44	−0.05	−0.02	0.50	0.023	−0.015	0.008
C2···C8^{VII}	1.698	0.047(1)	0.48(1)	−0.07	−0.02	0.58	0.027(1)	−0.021(1)	0.006(1)
	1.695	0.047	0.48	−0.07	−0.05	0.60	0.027	−0.021	0.006
C4···C4^{I}	1.734	0.034(1)	0.41(1)	−0.07	−0.02	0.48	0.022(1)	−0.015(1)	0.007(1)
	1.732	0.034	0.43	−0.07	−0.02	0.51	0.023	−0.016	0.007

[a] See Table 1 for the symmetry operations.

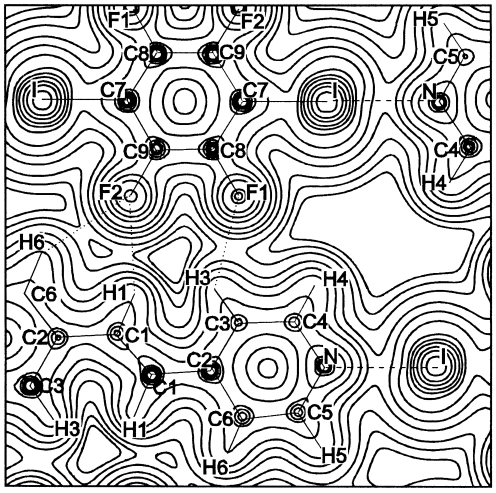

Figure 3. Experimental electron density, $\rho(r)$, in the same plane of Figure 2. The values of the contours (a.u.) increase from the outermost one inwards in steps of 2×10^n, 4×10^n, 8×10^n with n beginning at -3 and increasing in steps of 1.

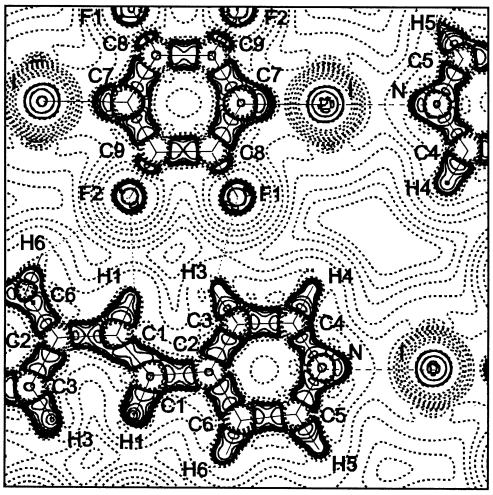

Figure 4. Laplacian, $\nabla^2\rho(r)$, of the experimental electron density map in the same plane as Figure 2. The absolute values of the contours (a.u.) are as in Figure 3. Positive values are denoted by dashed contours, negative values are denoted by solid contours.

formation enthalpy measured for a similar halogen-bonded system (i.e., the complex of 1-iodoperfluorohexane with 2,2,6,6-tetramethylpiperidine) is 7.5 kcal mol^{-1}.[23] Theoretical calculations at the DFT and MP2 levels on the $CF_3I\cdots NH_3$ dimer gave an interaction energy ΔE of 6.4 and 5.8 kcal mol^{-1}, respectively.[24] Our RHF and DFT calculations on the bpe·F_4DIB dimer gave $\Delta E = 3.6$ and 6.5 kcal mol^{-1}, respectively, for the experimental geometry, and 4.5 and 6.6 kcal mol^{-1}, respectively, for the optimized geometries. Walsh et al.[3] reported a ΔE value of 6.02 kcal mol^{-1} for the same dimer at the DFT level using a pseudopotential basis set. As consequence of these outcomes, it is evident that the I···N bond shows the same behavior as hydrogen bonds.

It is also evident that both the multipole and IAM models reproduce the effects of the intermolecular interactions well. In fact, their BCP properties are very similar for both models, as already outlined by Spackman,[25] revealing closed-shell character for all the interactions reported in Table 3. The only exception is the slight negative value of the local energy density E^e_b for the I···N bond from the POP + CUM model. As regards the IAM model, E^e_b is positive and close to zero. These observations suggest a very slight covalent character of the halogen bond.

The four C-H···F hydrogen bonds have ρ_b and $\nabla^2\rho_b$ values within the ranges 0.024–0.071 e Å^{-3} and 0.38-1.09 e Å^{-5}, respectively. The ρ_b and $\nabla^2\rho_b$ values of these hydrogen bonds

show a systematic decrease with the hydrogen to acceptor distance. Even if these ranges of values mark the limit of experimental accuracy, they are indicative of the relative strength of the hydrogen bonds.

The topology of $-\nabla^2\rho(r)$ for the complex bpe·F_4DIB indicates that the iodine and fluorine atoms are characterized by a torus of charge concentration perpendicular to the intramolecular bond. Each torus is slightly punctured on account of the formation of (3, −3) critical points that are far off the direction of the intermolecular interaction. This is in agreement with what can be deduced from the deformation density map (Figure 2b), in the regions of the I···N and F···H intermolecular bonds. Two (3, −3) critical points in the VSCCs associated with the C7 and N atoms ($\rho_b = 2.00$ e Å^{-3}, $-\nabla^2\rho_b = 35.7$ e Å^{-5} and $\rho_b = 3.93$ e Å^{-3}, $-\nabla^2\rho_b = 86.3$ e Å^{-5}, respectively) are very close to the line connecting the C7, I, and N atoms. Furthermore, these concentration maxima point toward the iodine valence-shell charge-depletion region which exhibits, in turn, two (3, +3) critical points (on average, $\rho_b = 0.34$ e Å^{-3}, $-\nabla^2\rho_b = -1.3$ e Å^{-5}) and nine (3, +1) saddle points (on average, $\rho_b = 0.37$ e Å^{-3}, $-\nabla^2\rho_b = -1.3$ e Å^{-5}) faced to the concentration maxima. This structure of the Laplacian appears to have a determining role in the relative alignment of the bpe and F_4DIB molecules in the crystal.[26]

A close examination of the shortest contacts in the crystal (i.e., with interatomic separations approximately within the van der Waals contact distance[13]) showed the presence of other weak interactions, as revealed by the existence of a bond path connecting the interacting atoms. The BCP properties of these interactions are reported at the bottom of Table 3. The F2···C4$_{x,\,y,\,1+z}$, C2···C8$_{-x,\,-y,\,-1-z}$, and C4···C4$_{-1-x,1-y,\,-1-z}$ contact distances (3.293(1), 3.379(1), and 3.469(1) Å, respectively) between adjacent molecules stacked along the *c* axis are indicative of π–π interactions between aromatic groups. Their bond paths are characterized by a strong curvature near the nuclear attractors.

Another short interatomic distance was found between the pair F2···F2$_{-1-x,\,-y,\,-z}$ (3.033(2) Å). This interaction connects F_4DIB molecules of different planes, shifted along the *a* axis. The presence of such F···F interactions can be interpreted as the consequence of a favorable energetic balance between them and the intermolecular interactions along the stacks (for example, π–π and hydrogen bonding), similar to what was observed in the pentafluorobenzoic acid.[27]

Experimental atomic charges: The atomic charges were determined by performing an integration over the topological atomic basins Ω[11] in the $\rho(r)$. A summation of the atomic volumes and electron populations reproduced the cell volume *V* and *F*(000) within 0.2 and 0.1%, respectively. The integrated Laplacian (L_Ω) was of the order of 10^{-2} e Å^{-2} for all types of atoms with the chosen level of accuracy, giving $L^{err} = (\Sigma_\Omega L^2_\Omega / N_{atoms})^{1/2} = 1.9 \times 10^{-2}$ e Å^{-2}. Thus, we are confident that the interatomic surfaces were determined with a good precision and that the integration results are reliable.

Table 4 shows the experimental net charges (*q*) of the bpe·F_4DIB complex. In the F_4DIB molecule ($q \cong -0.4$ e), the iodine atom is essentially neutral, the atom C7 is slightly negative ($q \cong -0.1$ e), the F atoms are negative ($q \cong -0.5$ e), and the carbon atoms bonded to them have an almost opposite net charge. In the bpe molecule ($q \cong 0.4$ e), the N atom and the ethylene group are highly negative, while the positive net charge is concentrated around the H and the other C atoms.

Table 4. Integrated net charge *q* [e] of the atomic basins Ω by the QTAM partitioning.

Ω	Experimental	Theoretical
I	−0.03	0.42
F1	−0.51	−0.75
F2	−0.50	−0.75
C7	−0.10	−0.25
C8	0.50	0.65
C9	0.44	0.64
N	−0.68	−1.59
C1	−0.22	0.05
C2	−0.02	−0.01
C3	0.13	0.13
C4	0.30	0.79
C5	0.27	0.86
C6	0.00	0.10
H1	0.19	−0.04
H3	0.08	−0.10
H4	0.17	−0.02
H5	0.05	−0.10
H6	−0.04	−0.08

The charge transfer of almost 0.4 e between bpe and F_4DIB molecules induces dipoles between adjacent molecules in the crystal that are most important in the formation of the halogen-bonded chains.

The charge distribution of the iodine atom is polarized towards the nitrogen atoms, so that its centroid is shifted in the direction of the C7 atom. In fact the dipole of the I atom is oriented towards the N atom and forms an angle of 9.1° with the I···N direction.

Comparison with theoretical topological analysis: The experimentally derived topological properties at the bond critical points were generally well reproduced by the theoretical calculations, in particular as far as the C7–I and I···N bonds are concerned (see Tables 2–4). The largest discrepancies concern the highly polar C–F bonds (see Table 2), as already evidenced in a previous charge density analysis of the pentafluorobenzoic acid,[27] where they were ascribed to the nature of the radial functions in the experimental model.[28] Our theoretical results also appear to be questionable for the highly positive Laplacian values at the critical points of the C–F bonds.

The comparison between experimental and theoretical net atomic charges (see Table 4) shows roughly a similar trend for the heavy atoms. However, the theoretical net charges of I and N atoms appear to be too high, probably as a consequence of the limited basis set and the absence of electron correlation in the RHF calculations. The total net charge on the F_4DIB molecule, $q = -0.08$, indicates that theory reproduced correctly, though in a lesser extent, the net charge transfer within the complex.

© 2003 WILEY-VCH Verlag GmbH & Co. KGaA, Weinheim
0947-6539/03/0907-1636 $ 20.00+.50/0 *Chem. Eur. J.* **2003**, *9*, No. 7

Conclusion

The present work gives a detailed description of chemical bonding in the bpe·F_4DIB charge-transfer complex in terms of electron density as determined by X-ray diffraction at 90 K and quantum mechanical calculations.

On the experimental side, we provide quantitative topological data for the electronic properties of the C–I and I···N halogen bonds that have not been reported in the literature so far. These two bonds are classified as closed-shell type. The C–I bond has topological features at the BCP which appear similar to those of metal–metal and metal–ligand bonds in organometallic compounds. We found a tight analogy in the electronic properties between the I···N halogen bonding and the hydrogen bonding. In particular, the BCP properties are very similar in magnitude to those of hydrogen bonds of medium strength.

The observed net charge transfer from bpe towards the F_4DIB molecule confirms the electrostatic character of the halogen bonding. The negative net charge is distributed among the fluorine and the iodine-bonded carbon atoms, and the positive charge is essentially localized on the carbon and hydrogen atoms of the pyridine group.

The sensitivity to crystal field effects of the electron density topology suggests that the I···N, F···H, F···F, F···C and C···C intermolecular interactions are significantly detectable.

The experimental results are fully confirmed by accurate theoretical calculations for both intramolecular and intermolecular (if available) BCP properties. The only discrepancies concern the topological properties of the polar bonds, as already evidenced in literature.

Experimental Section and Computational Details

Data collection and reduction: The synthesis and preparation of the crystals of the title compound were reported elsewhere.[3] The crystal used for data collection was glued onto a glass fiber with perfluorinated oil and slowly cooled to 90 K in a Kryoflex Bruker cooling device (N_2 gas stream). X-ray data were collected on a Bruker Smart Apex CCD area detector and data reduction was made with SAINT programs; absorption corrections based on multiscan were obtained by SADABS.[29] A summary of the experimental details is reported in Table 5.

Refinements: Three different refinements were carried out on $|F_o^2|$ by means of statistical weights. The VALRAY software[30] interfaced by one of us (R.B.) with the TOPOND program,[31] was used throughout.[32] The refinement results are summarized in Table 6. Refinement I is the conventional refinement (IAM model) of the positional parameters of all atoms, of anisotropic displacement parameters for I, F, N, and C atoms, and of isotropic ones for H atoms. Atomic scattering factors, including those for anomalous scattering of the I, N, and C atoms, were taken from *the International Tables for Crystallography* (**1995**, *Vol. C*). Refinement II in the IAM model also includes the third-order and fourth-order Gram–Charlier terms on the I atom (IAM + CUM model), which gave a very significant improvement in the modeling of X-ray data.

The atomic parameters from refinement II were used as starting values for the multipole refinement with the rigid pseudoatom model of Stewart.[10] The adopted aspherical model (POP + CUM) includes: the atomic positions and the mean-square amplitudes of vibration of I, F, N, and C pseudoatoms, third-order and fourth-order Gram–Charlier coefficients only on the iodine atom. The positions of H atoms were fixed to those obtained by a previous multipole refinement where the H atoms are polarized in the direction of the atom to which they are bonded, and only their isotropic thermal parameters were refined. For each heavy atom, the spherical core electron density and the valence deformation density is a sum of terms expressed by $C_{nlm}R_n(r)Y_{lm}(\theta, \phi)$, where C_{nlm} is a population parameter, $R_n(r)$ is a radial function of Slater type or a fixed linear combination of exponentials and $Y_{lm}(\theta, \phi)$ is a surface spherical harmonic. On the iodine atom position, functional expansions up to the hexadecapole level were introduced, whereas the expansions were broken at octapole level on the fluorine, nitrogen, and carbon positions, and at dipole level for the hydrogen atoms. For I, F, N, and C, the core- and valence-monopole scattering factors were calculated from Hartree–Fock atomic wave functions. A single parameter was refined for the core of all F, N, and C atoms. Each H monopole was a single shell, given by $\exp(-2.48\,r)$. As regards the higher multipoles, the Slater-type exponents (αs) of all the atoms were assigned fixed theory-based values.[33] Hirshfeld's rigid-bond test[34] was applied to the final thermal parameters. The r.m.s. of the mean-square displacement amplitude for bonded atoms along the bond vector in the title compound was 0.001 Å; therefore, the final model is consistent with the rigid-bond hypothesis.

Final atomic fractional coordinates, anisotropic, isotropic, cumulant thermal parameters, and multipole populations are given in the Supporting Information.

Table 5. Crystal data for bpe·F_4DIB.

chemical formula	$C_{18}H_{10}F_4I_2N_2$
chemical moieties	$(C_{12}H_{10}N_2 \cdot C_6F_4I_2)$
formula weight	584.08
dimensions [mm^3]	$0.25 \times 0.17 \times 0.11$
color, habit	colorless, prism
crystal system	triclinic
space group	$P\bar{1}$
a [Å]	6.2325(5)
b [Å]	8.2977(5)
c [Å]	9.0937(5)
α [°]	85.065(5)
β [°]	71.151(5)
γ [°]	79.259(5)
V [Å^3]	437.10(5)
Z	1
ρ_{calcd} [g cm^{-3}]	2.219
μ [mm^{-1}]	3.642
λ [Å], $Mo_{K\alpha}$	0.71073
diffractometer	Bruker Smart Apex
scan method	ϕ and ω
T [K]	90(2)
reflections for cell	19349
2θ range for cell reflections [°]	4.73–119.28
h, k, l range	−12/13, −18/18, 0/20
$2\theta_{max}$ [°]	109.67
no. of measured reflections	41661
no. of independent reflections	10025
R_{int}	0.0229
intensity decay	0.00
adsorption correction	Multiscan
transmission factors, T_{min}, T_{max}	0.891, 1.000

Table 6. IAM and multipole refinement information.

	IAM	IAM + CUM	POP + CUM
reflections with $\|F_o^2\| > 0$		9262	
number of parameters	129	154	386
$R(F)$	0.0223	0.0179	0.0153
$wR(F)$	0.0229	0.0189	0.0156
$R(F^2)$	0.0323	0.0240	0.0185
$wR(F^2)$	0.0440	0.0359	0.0292
S	1.423	1.164	0.958
k (scale factor)	0.9648(4)	0.9849(4)	0.987(2)
$(\text{shift/esd})_{max}$	0.01	0.01	0.01

Theoretical calculations: A first set of calculations were performed at the RHF level with the split valence SV2P basis set developed by Andzelm et al for the I atom,[35] and the 6-31G** basis set for the other atoms. In order to describe the strongest intermolecular interactions, calculations were performed on a cluster of one molecule of F_4DIB with the four nearest bpe molecules for the experimental low-temperature geometry. The wavefunction obtained through these calculations was used for the topological analysis of the electron density.

Other calculations were performed with the same basis set on the halogen-bonded dimer at the RHF and DFT level, with the experimental and the fully optimized geometries. From these calculations, we determined the interaction energy ΔE as the difference between the energy of the dimer and the sum of the energies of the single monomers. All the reported ΔE values were uncorrected for basis set superposition error. For DFT calculations, the B3LYP functional was used.[36, 37]

All the ab initio calculations were performed with the Gaussian 98 program.[38] The AIMPAC program[39] was used for the topological analysis of the electron density.

Acknowledgement

We thank Dr. C. Gatti and Dr. F. Cargnoni for useful discussions, and Prof. G. Resnati for the supply of crystals.

[1] G. R. Desiraju, R. L. Harlow, *J. Am. Chem. Soc.* **1989**, *111*, 6757 – 6764.
[2] a) A. C. Legon, *Chem. Eur. J.* **1998**, *4*, 1890 – 1897; b) A. C. Legon, *Angew. Chem.* **1999**, *111*, 2850 – 2880; *Angew. Chem. Int. Ed.* **1999**, *38*, 2687 – 2714.
[3] R. B. Walsh, C. W. Padgett, P. Metrangolo, G. Resnati, T. W. Hanks W. T. Pennington, *Cryst. Growth Des.* **2001**, *1*, 165 – 175.
[4] P. Metrangolo, G. Resnati, *Chem. Eur. J.* **2001**, *7*, 2511 – 2519.
[5] S. J. Garden, S. P. Fontes, J. L. Wardell, J. M. S. Skakle, J. N. Low, C. Glidewell, *Acta Crystallogr. Sect. B* **2002**, *58*, 701 – 709.
[6] A. S. Batsanov, A. J. Moore, N. Robertson, A. Green, M. R. Bryce, J. A. K. Howard, A. E. Underhill, *J. Mater. Chem.* **1977**, *7*, 387 – 389.
[7] J. Nishijo, E. Ogura, J. Yamaura, A. Miyazaki, T. Enoki, T. Takano, Y. Kuwatani, M. Iyoda, *Solid State Commun.* **2000**, *116*, 661 – 664.
[8] T. Devic, B. Domercq, P. Auban-Senzier, P. Molinié, M. Fourmigué, *Eur. J. Inorg. Chem.* **2002**, 2844 – 2849.
[9] J. P. M. Lommerse, A. J. Stone, R. Taylor, F. H. Allen, *J. Am. Chem. Soc.* **1996**, *118*, 3108 – 3116.
[10] R. F. Stewart, *Acta Crystallogr. Sect. A* **1976**, *32*, 565 – 574.
[11] R. F. W. Bader, *Atoms in Molecules - A Quantum Theory*; Oxford University Press: Oxford, **1994**.
[12] D. Phelps, A. Crihfield, J. Hartwell, T. W. Hanks, W. T. Pennington, R. D. Bailey, *Mol. Cryst. Liq. Cryst.* **2000**, *354*, 1111 – 1118.
[13] A. Bondi, *J. Phys. Chem.* **1964**, *68*, 441 – 451.
[14] V. R. Thalladi, H.-C. Weiss, D. Bläser, R. Boese, A. Nangia, G. R. Desiraju, *J. Am. Chem. Soc.* **1998**, *120*, 8702 – 8710.
[15] R. F. W. Bader, P. M. Beddall, *J. Chem. Phys.* **1972**, *56*, 3320 – 3329.
[16] Yu. A. Abramov, *Acta Crystallogr. Sect. A* **1997**, *53*, 264 – 272.
[17] E. Espinosa, E. Molins, C. Lecomte, *Chem. Phys. Lett.* **1998**, *285*, 170 – 173.
[18] R. Bianchi, G. Gervasio, D. Marabello, *Inorg. Chem.* **2000**, *39*, 2360 – 2366.
[19] R. Bianchi, G. Gervasio, D. Marabello, *Acta Cristallogr. Sect. B* **2001**, *57*, 638 – 645.
[20] R. Bianchi, G. Gervasio, D. Marabello, *Helv. Chim. Acta* **2001**, *84*, 722 – 734.
[21] E. Espinosa, M. Souhassou, H. Lachekar, C. Lecomte, *Acta Crystallogr. Sect. B* **1999**, *55*, 563 – 572.
[22] E. Espinosa, E. Molins, C. Lecomte, *Chem. Phys. Lett.* **1998**, *285*, 170 – 173.
[23] E. Corradi, S. V. Meille, M. T. Messina, P. Metrangolo, G. Resnati, *Angew. Chem.* **2000**, *112*, 1852 – 1856; *Angew. Chem. Int. Ed.* **2000**, *39*, 1782 – 1786.
[24] G. Valerio, G. Raos, S. V. Meille, P. Metrangolo, G. Resnati, *J.Phys. Chem. A* **2000**, *104*, 1617 – 1620.
[25] M. A. Spackman, *Chem. Phys. Lett.* **1999**, *301*, 425 – 429.
[26] T. S. Koritsanszky, P. Coppens, *Chem. Rev.* **2001**, *101*, 1583 – 1627.
[27] A. Bach, D. Lentz, P. Luger, *J.Phys. Chem. A* **2001**, *105*, 7405 – 7412.
[28] A. Volkov, C. Gatti, Yu. Abramov, P. Coppens, *Acta Crystallogr. Sect. A.* **2000**, *56*, 252 – 258.
[29] Bruker, *SMART*, *SAINT* and *SADABS*, Bruker AXS Inc., Madison, Wisconsin, USA, **1997**.
[30] R. F. Stewart, M. A. Spackman, C. Flensburg, *VALRAY*, versions **1995** and **2000**.
[31] C. Gatti, *TOPOND-98: an electron density topological program for systems periodic in N (N = 0 – 3) dimensions*, User's Manual, CNR-ISTM: Milano (Italy), **1999**.
[32] C. Gatti, R. Bianchi, *VALRAY95-TOPOND*, XXVI Congresso Nazionale Associazione Italiana di Cristallografia, Alessandria, Italy, September 1 – 4, **1996**, p. P139.
[33] W. J. Hehre, R. Ditchfield, R. F. Stewart, J. A. Pople, *J. Chem. Phys.* **1970**, *51*, 2769 – 2773.
[34] F. L. Hirshfeld, *Acta Crystallogr. Sect. A* **1976**, *32*, 239 – 244.
[35] J. Andzelm, M. Kłobukowski, E. Radzio-Andzelm, *J. Comp. Chem.* **1984**, *5*, 146 – 161.
[36] C. Lee, W. Yang, R. G. Parr, *Phys. Rev. B* **1988**, *37*, 785 – 789.
[37] A. D. Becke, *J. Chem. Phys.* **1993**, *98*, 5648 – 5652.
[38] M. J. Frisch, G. W. Trucks, H. B. Schlegel, G. E. Scuseria, M. A. Robb, J. R. Cheeseman, V. G. Zakrzewski, J. A. Montgomery, Jr., R. E. Stratmann, J. C. Burant, S. Dapprich, J. M. Millam, A. D. Daniels, K. N. Kudin, M. C. Strain, O. Farkas, J. Tomasi, V. Barone, M. Cossi, R. Cammi, B. Mennucci, C. Pomelli, C. Adamo, S. Clifford, J. Ochterski, G. A. Petersson, P. Y. Ayala, Q. Cui, K. Morokuma, D. K. Malick, A. D. Rabuck, K.Raghavachari, J. B. Foresman, J. Cioslowski, J. V. Ortiz, A. G. Baboul, B. B. Stefanov, G. Liu, A. Liashenko, P. Piskorz, I. Komaromi, R. Gomperts, R. L. Martin, D. J. Fox, T. Keith, M. A. Al-Laham, C. Y. Peng, A. Nanayakkara, M. Challacombe, P. M. W. Gill, B. Johnson, W. Chen, M. W. Wong, J. L. Andres, C. Gonzalez, M. Head-Gordon, E. S. Replogle, J. A. Pople, Gaussian 98, Revision A.9, Gaussian Inc., Pittsburgh, PA, **1998**.
[39] R. F. W. Bader, *AIMPAC: A set of programs for the theory of atoms in molecules*; McMaster University: Hamilton, Ontario (Canada), **1994**.

Received: October 23, 2002 [F4526]

 © 2003 WILEY-VCH Verlag GmbH & Co. KGaA, Weinheim